

Supporting Information

Coaxial Multi-shelled TiO₂ Nanotube Arrays for Dye Sensitized Solar Cells

Jijun Qiu¹, Fuwei Zhuge¹, Xiaomin Li^{1,*}, Xiangdong Gao¹, Xiaoyan Gan¹, Lin Li²,
Bingbing Wen², Zhisheng Shi^{2,*}, Yoon-Hwae Hwang³

¹ State Key Laboratory of High Performance Ceramics and Superfine Microstructures,
Shanghai Institute of Ceramics, Chinese Academy of Sciences, Shanghai 200050, China

² School of Electrical and Computer Engineering, University of Oklahoma, Norman,
Oklahoma 73019, USA

³ Department of Nano-Materials Engineering & BK 21 Nano Fusion Technology Division,
Pusan National University, Miryang 627-706, Korea

E-mail: Lixm@mail.sic.ac.cn, shi@ou.edu

Phone: 86-021-52412554, 01-405-525-4292

Contents:

Figure S1. The schematic fabrication procedure of LbL-AR for TiO₂ shells

Figure S2. The high-magnification FESEM images of ZnO spacing layer and multi-shelled TiO₂ NTs.

Figure S3. The typical FESEM and TEM images of multi-shelled TiO₂ NTAs with different shell numbers.

Figure S4. Typical high-magnification top-view FESEM images of broken tips of multi-shelled TiO₂ NTs with different shell numbers.

Figure S6. The typical characteristics of high-density triple-shelled TiO₂ NTAs.

Figure S6. The equivalent circuit model of the multi-shelled TiO₂ NTAs DSSCs.

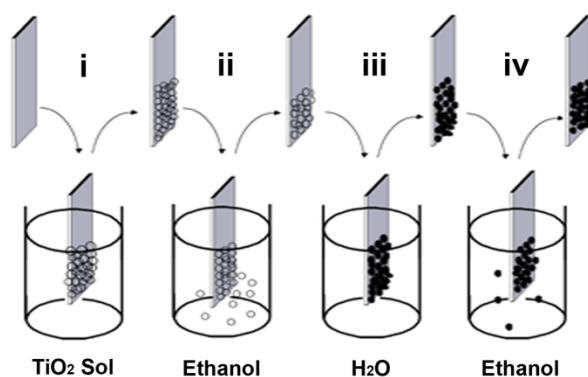


Figure S1. The schematic illustration for a cycle of LbL-AR procedure.

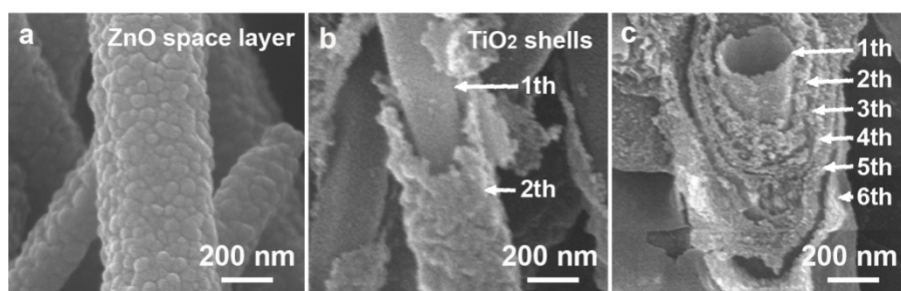


Figure S2. The high-magnification FESEM images of (a) ZnO space layer deposited over TiO₂ shells by SG technology, (b) double-shelled TiO₂ NT and (c) sextuple-shelled TiO₂ NTs.

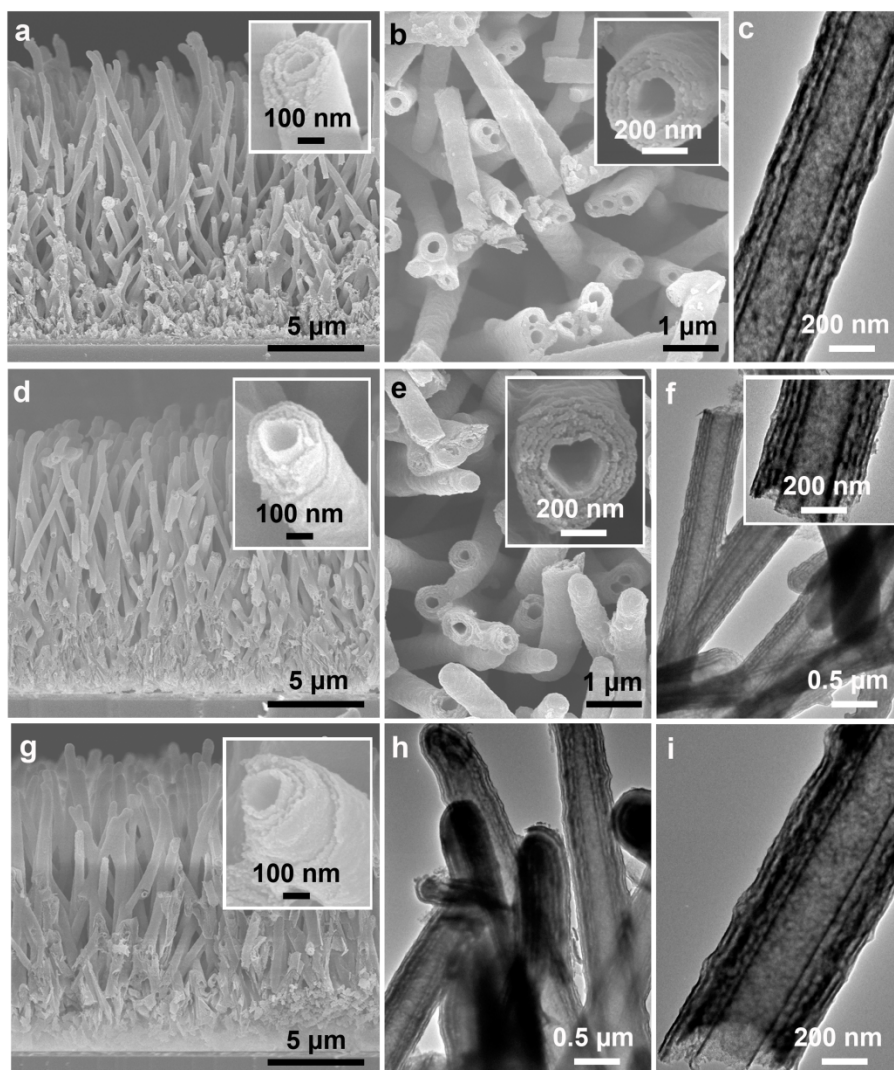


Figure S3. The typical FESEM and TEM images of multi-shelled TiO₂ NTAs with (a-c) quadruple, (d-f) quintuple- and (g-i) sextuple shells. Low-magnification side-view FESEM images of (a) quadruple, (d) quintuple and (g) sextuple-shelled TiO₂ NTAs. High-magnification top-view FESEM images of (b) quadruple- and (e) quintuple-shelled TiO₂ NTAs. Low-magnification TEM images of (f) quintuple- and (h) sextuple-shelled TiO₂ NTAs. High magnification TEM images of (c) quadruple- and (i) sextuple-shelled TiO₂ NTs.

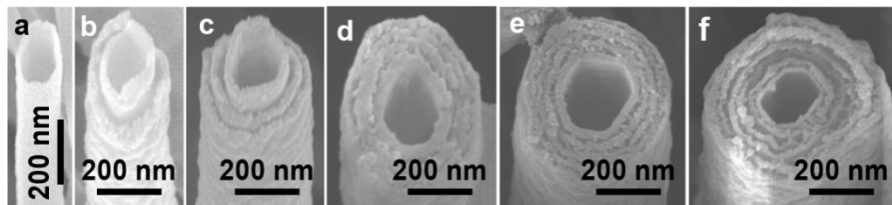


Figure S4. Typical high-magnification top-view FESEM images of broken tip of multi-shelled TiO₂ NTs with different shell numbers. (a) Single-, (b) double-, (c) triple-, (d) quadruple-, (e) quintuple- and (f) sextuple-shelled TiO₂ NT.

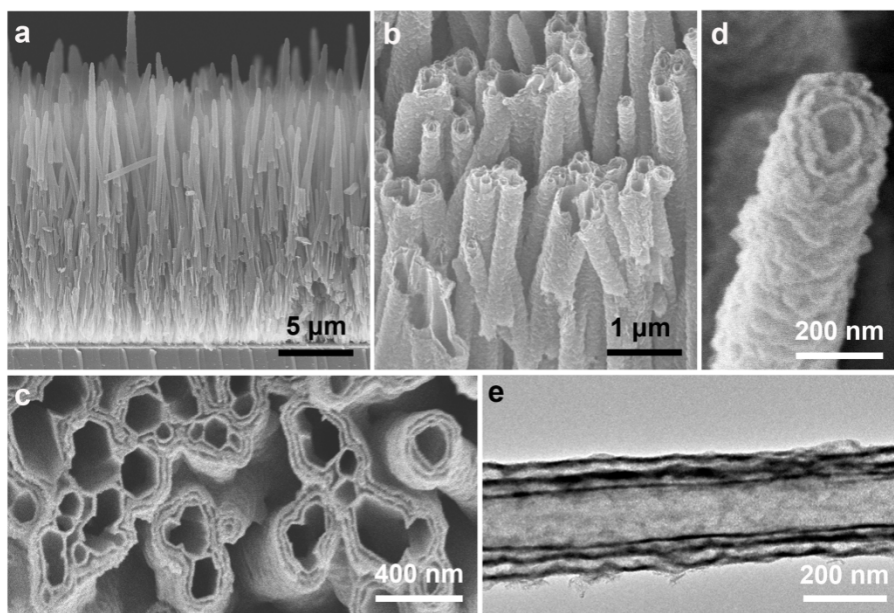


Figure S5. The typical characteristics of high-density triple-shelled TiO₂ NTAs. (a) low-, (b) middle magnification side-view FESEM images, (c) high magnification top-view FESEM image captured from broken edges of triple-shelled TiO₂ NTAs. (d) FESEM and (e) TEM images of an individual triple-shelled TiO₂ NT.

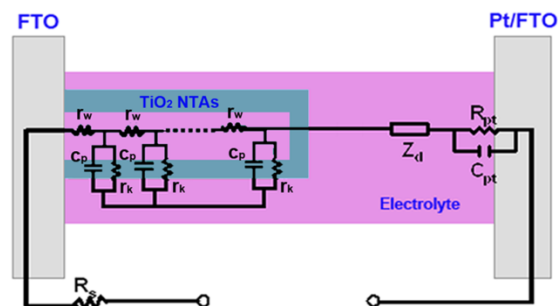


Figure S6. The equivalent circuit model of the multi-shelled TiO₂ NTAs DSSCs. The simulated electron transport parameters include the electron transport resistance ($R_w=r_wL$, r_w is component of the equivalent circuit, and L is the thickness of the multi-shelled TiO₂ NTAs photoanode), recombination resistance ($R_k=r_k/L$, r_k is component of the equivalent circuit), the capacitance of the electrical double layer ($C_p=c_pL$, c_p is component of the equivalent circuit), the electron collect efficiency ($\eta_{cc}=1- R_w/R_k$).